Efficient Transmission-Power-Control Scheme for Ku-Band High-Power Amplifiers in Portable User Earth Terminals

Hiroshi Okazaki, *Member, IEEE,* Takashi Ohira, *Senior Member, IEEE,* and Katsuhiko Araki

***Abstract*—A novel power-amplifier scheme is presented in this paper that realizes highly efficient transmission power control (TPC). The output power is controlled without sacrificing high power-added efficiency by combining multiple amplifiers with different power levels. Unique switching and impedance matching techniques make it possible to eliminate RF switching circuits and their associated power losses. This direct coupled architecture is called the "switchless amplifier-switching scheme." The requirements for realizing the novel power amplifiers used in this scheme are estimated, and Ku-band amplifier monolithic microwave integrated circuits (MMICs) that follow this scheme are fabricated. The capabilities of the scheme are confirmed by testing these MMICs. Finally, a novel power amplifier incorporating the developed MMICs is constructed to demonstrate its performance. Experimental results show that the amplifier can achieve a significant reduction in dc power at low output power levels under TPC.**

***Index Terms*—DC power reduction, high power amplifier, satellite communication, transmission power control.**

I. Introduction

THERE IS A growing demand for high-speed portable wireless terminals that offer rapid network access anywhere. A Ku-band multimedia satellite communication system has been proposed as one solution because it offers high transmission capacity and wide coverage area [1], [2]. The key component of the system is a high-speed user portable terminal. The terminal must be small, lightweight, and inexpensive, thus, low-power-consumption and high-cost-performance RF circuits are required. Among the terminal components, the high-power amplifier (HPA) consumes the most power. Thus, the HPA's efficiency must be improved for long battery operation.

The user terminal uses a small antenna with broad beamwidth. Therefore, the output power must be limited to ensure that it does not interfere with other radio communication systems. The propagation loss between the terminal and satellite depends on weather conditions, i.e., the well-known rain-attenuation effect. Thus, user terminals will require a transmission power control (TPC) function to handle rain attenuation; i.e., the output power has to be controlled so that it is low in clear weather and high in rainy weather. Since user terminals are mainly used in clear weather, the power consumption at low output power is a crucial factor and must be minimized.

This paper describes the efficient TPC scheme called the "switchless amplifier-switching scheme" and its performance estimation. It also describes the experimental results for a developed 25-dBm class Ku-band HPA. The TPC scheme makes it possible to construct low-power-consumption HPAs that are suitable for portable user terminals.

II. Conventional TPC Scheme

The TPC function is conventionally achieved through gain control at the preamplifier. The FETs or high electron-mobility transistors (HEMTs) in an HPA must be operated in the class-A or class-AB bias region at high frequencies, i.e., the Ku-band, to obtain useful gain. However, the input power range of an HPA with high power-added efficiency (PAE) is very narrow with class-A or class-AB operation. When the input power of the HPA is decreased for TPC, the efficiency drastically decreases. In other words, the HPA consumes dc power at almost a constant rate regardless of its output level. Thus, in the Ku-band, an HPA that employs a conventionally implemented TPC function wastes dc power in clear weather.

Another scheme for implementing the TPC function involves gain control of an HPA through bias voltage control of the devices. While gate bias voltage control causes linearity degradation, making it unsuitable for the TPC function, drain bias voltage control offers a compromise between efficiency and output power for HEMT HPAs [3], [4]. This latter scheme can expand the high PAE region. However, achieving real-time drain bias control with high efficiency for power supply is extremely difficult. It is also difficult to apply such a scheme to MESFET HPAs because the reflection coefficients of MESFETs vary greatly with drain voltage.

Switching among several HPAs that have been designed for different output levels is another way of realizing the TPC function in portable user earth terminals. Although this means that the HPA output takes discrete levels, this is enough to compensate the rain attenuation. An HPA configuration in which TPC is achieved by switching is shown in Fig. 1. Only one amplifier is set to the ON state at any one time. The switches are connected between input and output ports through the ON-state amplifier. Since switches are used, there is a major tradeoff between the insertion loss and the isolation of the switch at high frequencies. In particular, the insertion loss of the output switch directly degrades the overall efficiency.

Manuscript received February 1, 2000.

H. Okazaki and K. Araki are with the NTT Network Innovation Laboratories, Yokosuka 239-0847, Japan (e-mail: okazaki@wslab.ntt.co.jp).

T. Ohira is with the ATR Adaptive Communications Research Laboratories, Kyoto 619-0288, Japan.

Publisher Item Identifier S 0018-9480(01)04437-4.

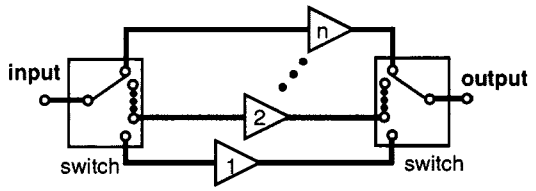

Fig. 1. HPA configuration in which TPC is achieved by switching among several amplifiers.

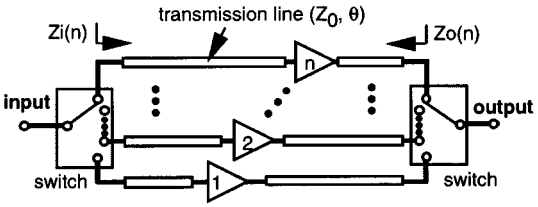

Fig. 2. Improved HPA configuration with transmission lines.

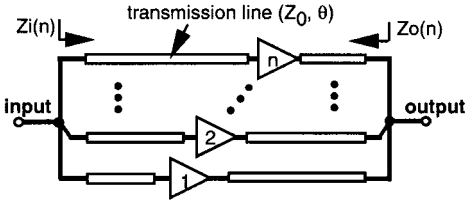

Fig. 3. Switchless HPA configuration.

III. Switchless Amplifier-Switching Scheme

A technique that improves the isolation and a solution to the tradeoff problem were briefly reported in [5]. Both can be achieved by putting transmission lines between the switch and the amplifier, as shown in Fig. 2. The input or output impedance of each amplifier from the switch $Zi(n)$ or $Zo(n)$ varies with transmission-line length. Since the transmission lines' characteristic impedances Z_0 are matched to the amplifier's input and output impedance, transmission line length θ does not affect the ON-state impedance of the amplifier. The OFF-state input or output impedance of an amplifier differs from its ON-state impedance. If the conductor loss of the transmission line is low, the impedance variation due to transmission-line length is maxim at the point where the angle of the s-parameter equals zero at a target frequency. It follows that when the length of the transmission line is determined so as to maximize the OFF-state input or output impedance of each amplifier, including the transmission line, the isolation at the switch is improved. This allows the use of low-insertion-loss switches.

If the impedances of all branches, except the ON-state amplifier, approach infinity, the switches can be removed, which realizes a novel HPA with the TPC function. This HPA configuration, called the "switchless configuration," is shown in Fig. 3. An HPA with the switchless configuration is expected to have the advantages of lower cost, lower insertion loss, and greater power-handling capability because it does not use the RF switches of the conventional switching scheme. To realize this novel HPA, the matching circuit design should ensure high efficiency and output power, and large mismatch in the OFF state.

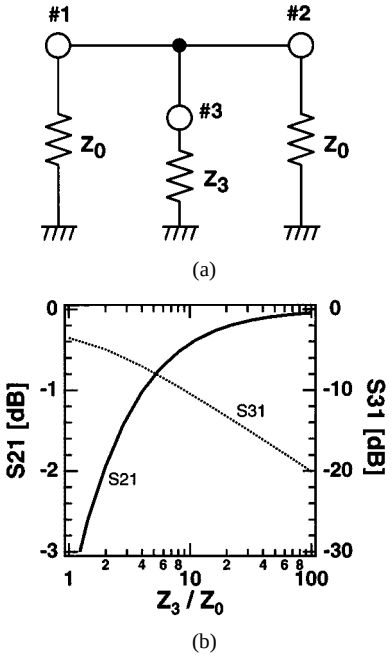

Fig. 4. Loss and leakage estimations for the switchless configuration. (a) Circuit diagram. (b) Simulation results.

The requirements for the switchless switching amplifier scheme were estimated. Fig. 4(a) shows the circuit diagram and Fig. 4(b) shows the simulation results. The load impedances at ports 1–3 are Z_0, Z_0, and Z_3, respectively. $S21$ shows the ratio of port-2 output to port-1 input. Z_3 is the input impedance of the OFF-state amplifier, including the transmission line. Since the maximized impedance is obtained at the point where the angle of the s-parameter equals zero, the imaginary part of the impedance equals zero. Therefore, the load impedance was treated as resistance in this simulation. The results of $S21$ show that low-insertion loss is achieved with high Z_3 values. Z_3 has to be more than four times Z_0 to hold the insertion loss to under 1.0 dB. $S31$ shows the ratio of leakage to port-3 to port-1 input. The $S31$ results show that leakage to the OFF-state amplifier is low if Z_3 is high. Therefore, high power-handling capability is also achieved with high Z_3.

IV. Performance Estimation with Fabricated MMICs

Three different amplifier MMICs were fabricated with a 0.5-μm GaAs MESFET process to provide 5 dB of TPC. They have a common-source configuration. Their matching circuits were simultaneously optimized by gain matching at the class-A bias point, where drain current ($I\mathrm{ds}$) is 0.6 times the saturated drain current, and by impedance mismatching in the pinchoff region, where $I\mathrm{ds}$ is zero. Fig. 5 shows the gate bias voltage ($V\mathrm{gs}$) versus $I\mathrm{ds}$ characteristics of a typical FET. The gatewidth is 1.6 mm. Pinchoff occurs when $V\mathrm{gs}$ is less than -1.7 V. Thus, the pinchoff bias voltage was set to -2.0 V for each amplifier.

Two of the amplifiers ($AL1$ and $AL2$) have a gatewidth of 0.4 mm and were designed to achieve 20 dBm of saturated output power ($P\mathrm{sat}$). The other ($AH1$) has a gatewidth of 1.6 mm and was designed for a $P\mathrm{sat}$ of 25 dBm. The drain bias voltage ($V\mathrm{ds}$) was set to 10.8 V in each amplifier during all

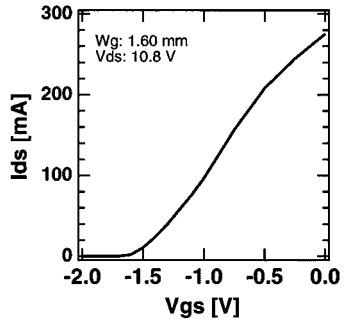

Fig. 5. Vgs–Ids characteristics of a typical FET.

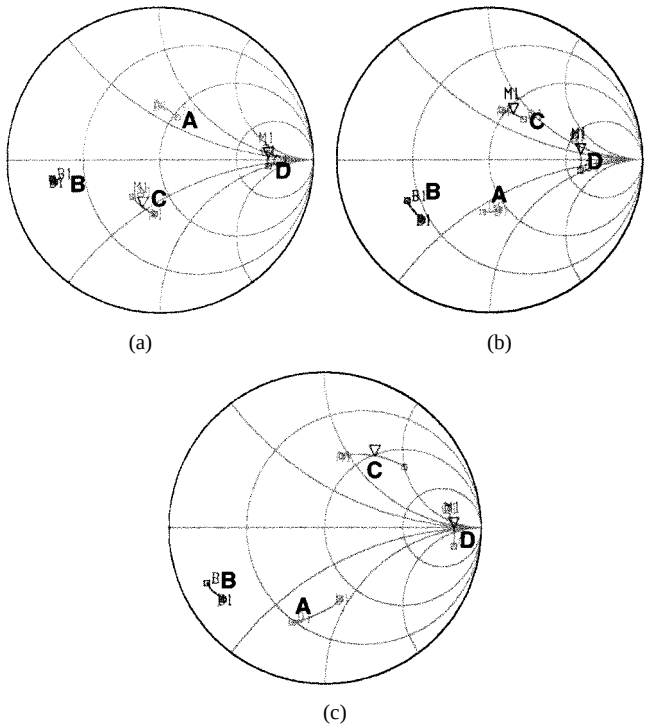

Fig. 6. Reflection coefficients of the developed Ku-band amplifier MMICs. (a) $S11$ of $AL2$. (b) $S22$ of $AL2$. (c) $S22$ of $AH1$. A: ON-state reflection coefficient. B: OFF-state reflection coefficient. C: simulated ON-state reflection coefficient with the transmission line. D: simulated OFF-state reflection coefficient with the transmission line.

measurements. Each amplifier is switched on or off by using the gate-bias switching method, which switches the gate bias between the class-A bias region and the pinchoff bias region. This method is simpler and more reliable than drain-bias switching and can be used with the burst-mode operation technique [6].

Fig. 6(a)–(c) shows examples of the variation in the reflection coefficient of the fabricated amplifier MMICs. Fig. 6(a) and (b) shows the input reflection coefficient ($S11$) and output reflection coefficient ($S22$) of $AL2$ at frequencies between 14.0–14.5 GHz, respectively. Fig. 6(c) shows the $S22$ of $AH1$ for the same frequency band. A–D in each figure are the measured ON-state reflection coefficient, measured OFF-state reflection coefficient, simulated ON-state reflection coefficient with the transmission line, and simulated OFF-state reflection coefficient with the transmission line, respectively. Each MMIC's OFF-state reflection coefficient (i.e., B) became high

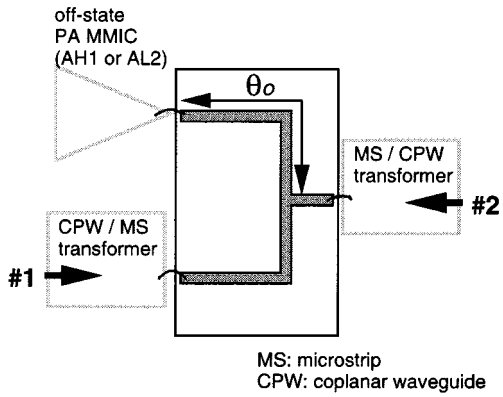

Fig. 7. Layout of the test circuit.

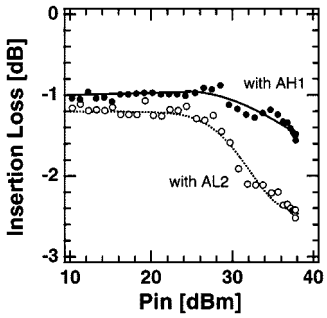

Fig. 8. Insertion loss of the test circuits.

due to the inclusion of the appropriate transmission line D. The results were $6Z_0$ for $S11$ of $AL2$, $4Z_0$ for $S22$ of $AL2$, and $10Z_0$ for $S22$ of $AH1$ with 105°, 115°, and 115° transmission lines, respectively. The results for $AL1$ were nearly same as $AL2$. Thus, the three fabricated amplifier MMICs with transmission lines were able to fulfill the switchless configuration requirements described in the previous section.

Two test circuits containing a fabricated amplifier MMIC ($AL2$ or $AH1$) were constructed to measure the performance of the switchless scheme (Fig. 7). The transmission lines were realized as microstrip lines on 380-μm-thick alumina substrates. The length of the microstrip lines, θo, was 90° at 14.25 GHz (2.04 mm) for both MMICs. This value was determined by the method outlined in Section III, and the difference from the previous value is due to the consideration of bonding wire length. The insertion losses at various input powers at 14.25 GHz are shown in Fig. 8. The insertion losses at low-input levels with $AH1$ and $AL2$ are 1.0 and 1.2 dB, respectively. They include the loss of lines, wiring, and the transformers between the microstrip line and the coplanar waveguide. The measured results agree well with the simulation results shown in Fig. 4(b). The insertion loss degrades at higher input power levels because the excess leakage to the MMIC alters the OFF-state reflection coefficient of the MMIC. It is constant if the input power is less than 26 dBm for the test circuit with $AL2$ and 30 dBm for the test circuit with $AH1$. This means that the switchless configuration gives the fabricated MMICs the power-handling capability of 5–6 dB over the OFF-state amplifier's $P\mathrm{sat}$. $Pi(1\mathrm{dB})$, the input power where the insertion loss increases by 1 dB compared to the

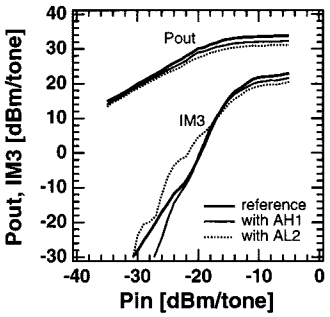

Fig. 9. Two-tone test results from the test circuits.

insertion loss at lower input levels, is an important factor in switches. The $Pi(1\text{dB})$ of the test circuit with $AL2$ is 32 dBm; for the one with $AH1$, we estimate the value to be 42 dBm.

Excess leakage often causes intermodulation within the MMIC devices. Fig. 9 shows the results of two-tone measurements with a 37-dBm-class amplifier and the test circuit connected at the output port of the amplifier. The input frequencies were 14.250 and 14.251 GHz. The characteristics of the amplifier without the test circuit are also shown for reference. Although some increase in third-order intermodulation products (IM3) with $AL2$ are observed, they are small at required output power levels of less than 22 dBm per tone. These results show that the switchless configuration has the ability to handle 25 dBm of output power with low insertion loss.

V. Experimental Results and Discussions

A. Input or Output Switchless Configuration

Fig. 10(a) shows a block diagram of the circuit constructed to confirm the performance of the input switchless configuration. The microstrip transmission line was constructed on a 380-μm-thick alumina substrate. Line lengths, $\theta i(h)$ and $\theta i(l)$, were determined to be 90° (2.04 mm) and 95° (2.14 mm) for $AL1$ and $AL2$ at 14.25 GHz, respectively. They were calculated considering the bonding wire length. Fig. 10(b) shows the measured input–output characteristics at 14.25 GHz. Due to the limitation of the measurement system, the output port of the OFF-state MMIC chip was open. The results were similar to those for the MMICs. The difference, less than 0.5 dB of gain degradation, was due to the insertion loss with the switchless configuration.

Measurements to confirm the performance of output switchless configuration were also carried out using the circuit shown in Fig. 11(a). Microstrip transmission lines length $\theta o(h)$ and $\theta o(l)$ was determined to be 90° at 14.25 GHz (2.04 mm) for both $AL2$ and $AH1$. They were again calculated considering the bonding wire length. The circuit has two input ports. When the signal is input to "input1," the lower amplifier ($AL2$) is off and the upper one ($AL2 + AH1$) is on, while when the signal is input to "input2," the lower one is on and the upper one is off. The input port of the OFF-state amplifier was open for the same reason described above. Fig. 11(b) and (c) shows the measured input–output characteristics and PAE for each case at 14.25 GHz. The characteristics of the final-stage amplifier

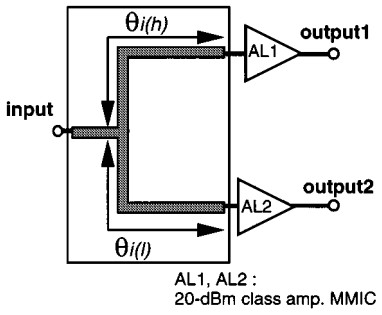

(a)

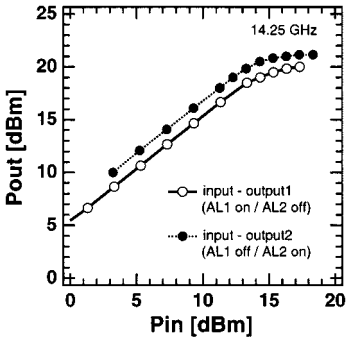

(b)

Fig. 10. Input–output characteristics of the circuit with the input switchless configuration. (a) Block diagram. (b) Results.

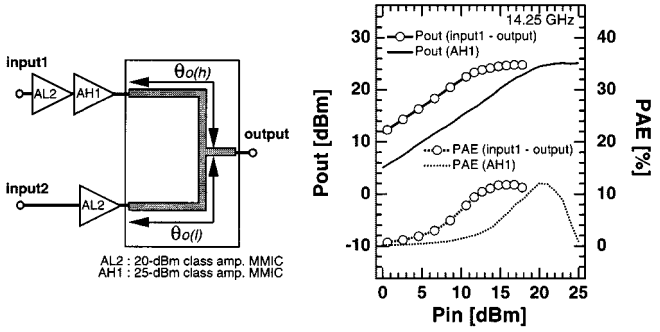

(a) (b)

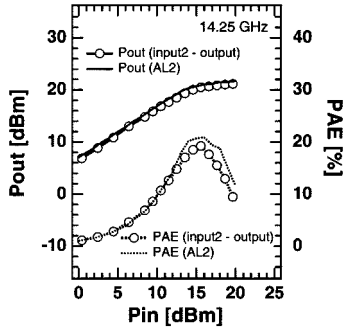

(c)

Fig. 11. Input–output characteristics of the circuit with the output switchless configuration. (a) Block diagram. (b) Results (input1–output). (c) Results (input2–output).

MMICs $AH1$ and $AL2$ are also shown for comparison. The results were similar to those for the MMICs, except for a slight degradation in gain and output power.

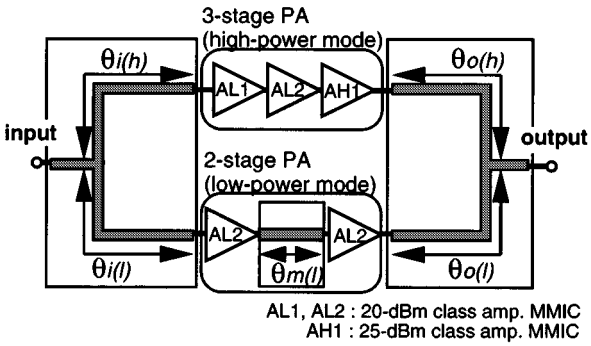

(a)

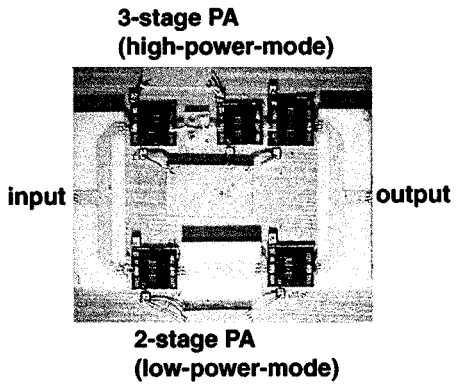

(b)

Fig. 12. Fabricated HPA with the switchless configuration. (a) Block diagram. (b) Photograph.

B. Input and Output Switchless Configuration

Fig. 12 depicts a block diagram and photograph of the HPA with the input and output switchless configuration. The HPA consists of two- and three-stage amplifiers. The input and output transmission lines used are described in Section V-A. In the high-power mode, the two-stage amplifier is off and the three-stage one is on, while in the low-power mode, the two-stage amplifier is on and the three-stage one is off.

A transmission line was set in the middle of the two-stage amplifier to increase its stability in the high-power mode. It was a 50-Ω microstrip transmission line on a 380-μm-thick alumina substrate. The length of the line, i.e., $\theta m(l)$, was determined to be 90° at 14.25 GHz (2.04 mm) so as to ensure that the clockwise loop leakage had phase opposite to that of the input signal. Using the line increases the stability of the HPA, although there is some gain degradation in the high-power mode. The HPA was stable during the following measurements in both modes.

The measured frequency responses of high- and low-power modes are shown in Fig. 13(a) and (b), respectively. In the high-power mode, the gain $S21$ was between 14.2–14.7 dB for frequencies between 14.0–14.5 GHz. In the low-power mode, it was between 10.9–11.9 dB for the same frequency band.

The input–output characteristics and dc power consumption of each mode are shown in Fig. 14. The measured frequency was 14.25 GHz. The output powers of the 1-dB gain compression point ($\mathrm{P}_{1\,dB}$) of the high- and low-power modes were 24.5 and 18.8 dBm, respectively. The power consumption of the high- and low-power modes at $\mathrm{P}_{1\,\mathrm{dB}}$ were 2.52 and 0.71 W, respectively. Due to the gain degradation in the high-power mode be-

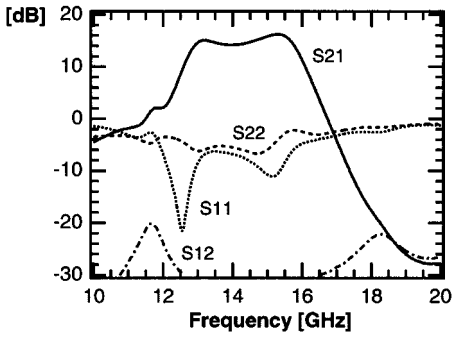

(a)

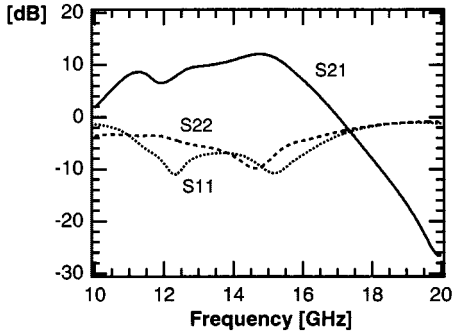

(b)

Fig. 13. Frequency response of the HPA. (a) High-power mode. (b) Low-power mode.

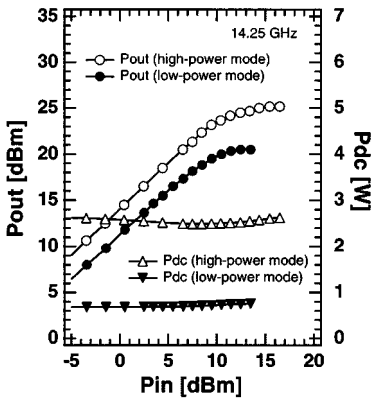

Fig. 14. Input–output characteristics and dc power consumption ($P\mathrm{dc}$).

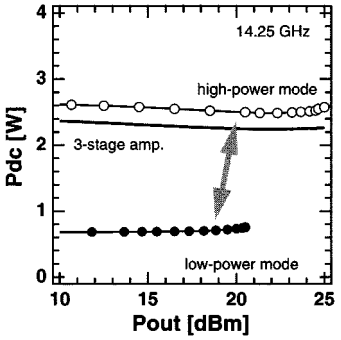

Fig. 15. Power consumption of the HPA and three-stage amplifier.

cause of the use of the additional transmission line for stability, the HPA had 3 dB of TPC range with amplifier switching only. However, we were able to expand the range of TPC to 5.7 dB

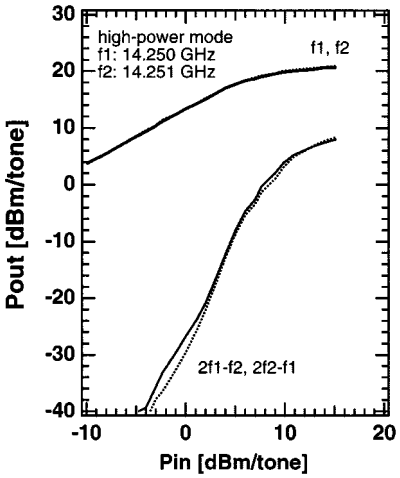

(a)

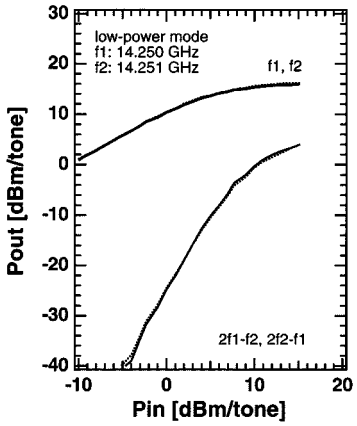

(b)

Fig. 16. Two-tone test results of the HPA. (a) High-power mode. (b) Low-power mode.

(under 18.8 and 18.8–24.5 dBm) using the proposed scheme along with gain control at the preamplifier; this reduced the HPA's power consumption by 72%. To precisely confirm the dc power reduction effect, the three-stage amplifier, shown in Fig. 12, was constructed and measured. The $V\mathrm{ds}$ of the amplifier was reduced to 10.0 V to set the output at $\mathrm{P}_{1\,\mathrm{dB}}$ to 24.5 dBm. Fig. 15 shows the dc power consumption at various output levels for the three-stage amplifier and HPA. The power consumption of the three-stage amplifier at 24.5 and 18.8 dBm was the same, i.e., 2.26 W. Thus, the dc power reduction of the HPA is estimated to be 69%. The dc power consumption could be reduced even further if the MMICs were designed by a more efficient technique such as load–pull instead of gain–match.

Fig. 16(a) and (b) shows the results of two-tone measurements in the high- and low-power modes, respectively. The input frequencies were 14.250 and 14.251 GHz, respectively. No significant IM3 effects were observed. These results confirm the power-handling capability of the off-state MMICs, as estimated in Section IV.

VI. Conclusion

A switchless amplifier-switching scheme that minimizes the dc power consumption of HPAs at low-power output under TPC has been described in this paper. The scheme has the advantages of lower cost, lower insertion loss, and better power-handling capability than the conventional switching scheme because it eliminates RF switches by using short-length transmission lines. Ku-band amplifier MMICs were designed and found to satisfy the proposed scheme's requirements. MMICs were fabricated and found to offer insertion losses under 1.2 dB at input power levels of less than 26 dBm. Amplifier MMICs and transmission lines were used to construct a 25-dBm class HPA, in which the TPC function was achieved by activating the two amplifiers selectively. The HPA demonstrated 5.7 dB of TPC and a 70% dc power reduction in the low-power mode. Since it can provide TPC while minimizing HPA power consumption, it will yield very efficient portable user terminals for satellite communication systems.

Acknowledgment

The authors wish to thank K. Maruyama, NTT Electronics Corporation, Atsugi, Japan, for his help with the measurements, and Dr. H. Mizuno, NTT Network Innovation Laboratories, Yokosuka, Japan, for his continuous encouragement.

References

[1] M. Nakayama, K. Araki, M. Kobayashi, and H. Nakashima, "A satellite communication system using a ATM multiplex scheme for interactive multimedia networks," presented at the 48th Int. Astronaut. Congr., 1997, paper IAF-97-M.2.10.

[2] H. Kazama, K. Kobayashi, T. Otsu, and K. Araki, "Spread spectrum FDMA over high speed TDM transmission system for multimedia satellite communications," in *Proc. IEEE 5th Int. Spread-Spectrum Tech. Applicat. Symp.*, 1998, pp. 714–718.

[3] A. Platzker and S. Bouthillette, "Variable output, high efficiency-low distortion S-band power amplifiers and their performances under single tone and noise power excitations," in *IEEE MTT-S Int,. Microwave Symp. Dig.*, 1995, pp. 441–444.

[4] S. Bouthillette and A. Platzker, "High efficiency L-band variable output power amplifiers for use in communication systems," in *IEEE MTT-S Int. Microwave Symp. Dig.*, 1996, pp. 563–566.

[5] H. Okazaki, T. Ohira, and K. Araki, "Efficient high power amplifiers with transmission power control function," in *29th European Microwave Conf.*, vol. 2, 1999, pp. 275–278.

[6] H. Okazaki, K. Horikawa, and M. Tanaka, "Ku-band self-controlled burst mode high power amplifier," in *IEEE MTT-S Int. Microwave Symp. Dig.*, 1994, pp. 557–560.

Hiroshi Okazaki (A'94–M'00) was born in Okayama, Japan, in 1965. He received the B.E. and M.E. degrees from Osaka University, Osaka, Japan, in 1988 and 1990, respectively.

In 1990, he joined the Nippon Telegraph and Telephone (NTT) Corporation, Yokosuka, Japan, where he has been involved in the investigation of low-power-consumption solid-state power amplifiers (SSPAs) for earth stations at the NTT Radio Communication Systems Laboratories. Since 1993, he has been involved with research on microwave circuit techniques for monolithic integration. He is currently a Senior Research Engineer at the NTT Network Innovation Laboratories, Yokosuka, Japan, where he is engaged in development of RF equipment for satellite communication.

Mr. Okazaki was the recipient of the 1997 Young Engineer Award presented by the Institute of Electronics, Information and Communication Engineers (IEICE), Japan and the 1998 Japan Microwave Prize.

Takashi Ohira (S'79–M'80–SM'99) was born in Osaka, Japan, in 1955. He received the B.E. and D.E. degrees in communication engineering from the Osaka University, Osaka, Japan, in 1978 and 1983, respectively.

In 1983, he joined the NTT Electrical Communication Laboratories, Yokosuka, Japan, where he was engaged in research on monolithic integration of microwave semiconductor devices and circuits. He developed GaAs MMIC transponder modules and microwave beam-forming networks (BFNs) aboard Japanese domestic multibeam communication satellites, ETS-VI, and ETS-VIII, at NTT Wireless Systems Laboratories, Yokosuka, Japan. Since 1999, he has been engaged in research on microwave analog adaptive antennas at ATR Adaptive Communications Research Laboratories, Kyoto, Japan. He co-authored *Monolithic Microwave Integrated Circuits* (Tokyo, Japan: IEICE, 1997).

Dr. Ohira is the IEEE Microwave Theory and Techniques Society (IEEE MTT-S) Japan Chapter vice-chairperson. He was the recipient of the 1986 Shinohara Prize and the 1998 Japan Microwave Prize.

Katsuhiko Araki received the B.E. and M.E. degrees from the Tokyo Institute of Technology, Tokyo, Japan, in 1979 and 1981, respectively.

In 1981, he joined the NTT Electrical Communications Laboratories, Yokosuka, Japan, during which time he was engaged in research on GaAs monolithic microwave circuits and involved with the development of communication satellite onboard transponders. He is currently a Senior Research Engineer, Supervisor at NTT Network Innovation Laboratories, Yokosuka, Japan.

Mr. Araki is a member of the American Institute of Aeronautics and Astronautics (AIAA) and the Institute of Electronics, Information and Communication Engineers (IEICE), Japan. He was the recipient of the 1988 Shinohara Prize.